J|A|C|S
ARTICLES
Published on Web 03/13/2007

Nephila clavipes Spider Dragline Silk Microstructure Studied by Scanning Transmission X-ray Microscopy

Marie-Eve Rousseau,[†] Daniel Hernández Cruz,[‡] M. Marcia West,[‡] Adam P. Hitchcock,[‡] and Michel Pézolet*,[†]

Contribution from the CERSIM, CREFSIP, Département de Chimie, Université Laval, Québec, Canada G1K 7P4, and the Department of Chemistry, McMaster University, Hamilton, Ontario, Canada L8S 4M1

Received October 23, 2006; E-mail: michel.pezolet@chm.ulaval.ca

Abstract: *Nephila clavipes* dragline silk microstructure has been investigated by scanning transmission X-ray microscopy (STXM), a technique that allows quantitative mapping of the level of orientation of the peptide groups at high spatial resolution (<50 nm). Maps of the orientation parameter $\langle P_2 \rangle$ have been derived for spider silk for the first time. Dragline silk presents a very fine microstructure in which small, highly oriented domains (average area of 1800 nm^2, thus clearly bigger than individual β-sheet crystallites) are dispersed in a dominant, moderately oriented matrix with several small unoriented domains. Our results also highlight the orientation of the noncrystalline fraction in silk, which has been underestimated in numerous structural models. No evidence of either a regular lamellar structure or any periodicity along the fiber was observed at this spatial resolution. The surface of fresh spider silk sections consists of a ~30−120 nm thick layer of highly oriented protein chains, which was found to vary with the reeling speed, where web building (0.5 cm/s) and lifeline (10 cm/s) spinning speeds were investigated. While the average level of orientation of the protein chains is unaffected by the spinning speed, STXM measurements clearly highlight microstructure differences. The slowpull fiber contains a larger fraction of highly oriented domains, while the protein chains are more homogeneously oriented in the fastpull fiber. In comparison, cocoon silk from the silkworm *Bombyx mori* presents a narrower orientation distribution. The strength−extensibility combination found in spider dragline silk is associated with its broad orientation distribution of highly interdigitated and unoriented domains.

Introduction

Spiders have evolved to become experts regarding silk production. Orb-weaving spiders, *Nephila clavipes* in particular, spin many different types of silk fibers, each with a specific range of mechanical properties.[1,2] Dragline silk, the silk commonly investigated and best understood so far, exhibits high toughness that comes from a good trade-off between stiffness and extensibility. This type of silk is used by the orb-weaving spiders for multiple functions which require different mechanical properties that can be modulated by varying the spinning speed.[3,4] When used as a lifeline to escape a predator, dragline silk is spun at high speed (≥10 cm/s), which produces a stiff fiber that can support the spider's own body weight during its vertical descent. On the other hand, the web frame is spun several orders of magnitude slower (≤1 cm/s), which leads to a tough yet extensible thread that will support the distorting forces induced by wind and rain as well as cooperate with the capture spiral to dissipate the kinetic energy transferred to the web when a flying prey is being captured.[5,6]

The microstructure of the silk filament, which is directly linked to its mechanical properties, is influenced by the primary structure of the protein as well as the processing conditions. The protein feedstock stored in the spider's major ampullate gland, where dragline spidroin synthesis takes place, is extruded in a complex spinning apparatus where pH and concentration of specific ions are varied judiciously to allow chain interactions and elimination of excess water.[7] Protein assembly and prealignment is further ensured by the nematic liquid crystalline state occurring in the duct.[8,9] Prior to fiber extrusion, a rapid extensional flow induces chain alignment and conformational changes[10] that are further optimized by draw-down crystalliza-

[†] Université Laval.
[‡] McMaster University.

(1) Gosline, J. M.; Demont, M. E.; Denny, M. W. *Endeavour* **1986**, *10*, 37−43.
(2) Vollrath, F.; Porter, D. *Soft Matter* **2006**, *2*, 377−385.
(3) Thiel, B. L.; Viney, C. *J. Microsc. (Oxford, U.K.)* **1997**, *185*, 179−187.
(4) Vollrath, F.; Madsen, B.; Shao, Z. Z. *Proc. R. Soc. London, Ser. B* **2001**, *268*, 2339−2346.
(5) Gosline, J. M.; Lillie, M.; Carrington, E.; Guerette, P.; Ortlepp, C.; Savage, K. Elastomeric Proteins: Structures, Biomechanical Properties, and Biological Roles. In *Elastic Proteins: Biological Roles and Mechanical Properties*; Shewry, P. R., Tatham, A. S., Bailey, A. J., Eds.; Cambridge University Press: Cambridge, U.K., 2003; pp 15−38.
(6) Vollrath, F.; Porter, D. *Appl. Phys. A* **2006**, *82*, 205−212.
(7) Vollrath, F.; Knight, D. P. *Nature* **2001**, *410*, 541−548.
(8) Knight, D. P.; Vollrath, F. Elastomeric Proteins: Structures, Biomechanical Properties, and Biological Roles. In *Biological Liquid Crystal Elastomers*; Shewry, P. R., Tatham, A. S., Bailey, A. J., Eds.; Cambridge University Press: Cambridge, U.K., 2003; pp 302−320.
(9) Knight, D.; Vollrath, F. *Biomacromolecules* **2001**, *2*, 323−334.
(10) Knight, D. P.; Knight, M. M.; Vollrath, F. *Int. J. Biol. Macromol.* **2000**, *27*, 205−210.

tion occurring ex vivo.[11] Consequently, the conformation of the proteins, the chain assembly into supramolecular structures, as well as the molecular orientation at different length scales will all be influenced by the spinning conditions and will have an impact on the mechanical properties of the resulting silk thread. A detailed understanding of silk microstructure is highly motivated by industrial efforts to produce synthetic fibers that biomimic spider silk's strength and toughness. Achievement of this goal requires the combination of several characterization techniques to fully unravel the organization of proteins in silk fibers.

There is ample experimental evidence to show that silk is a material with a hierarchical organization. Described as a semicrystalline biopolymer, the unique combination of mechanical properties of spider dragline silk has inspired models in which interconnected crystalline and amorphous rubbery regions are responsible for the silk's high strength and extensibility, respectively.[1,12] Small oriented crystalline inclusions ($5 \times 2 \times 6$ nm^3),[13] principally made of repetitive poly(alanine) sequences that adopt the antiparallel β-sheet conformation,[14] have been found. The noncrystalline counterpart contains glycine-rich domains that preferentially adopt the β-sheet conformation and a 3-fold helical structure.[15,16] The so-called amorphous matrix was best characterized by a glassy state in dry silk with organized and oriented chains[16] that gain a rubbery character when plasticized by water.[1,2] Due to the small crystalline fraction of dragline silk (<15%)[13] associated with the poly(alanine) sequences, a three-phase model that considers an oriented noncrystalline interphase around the crystallites was found to be appropriate to account for spider silk's high strength.[13,17] Nanofibrils[18−21] composed of crystalline and short-range ordered domains have also been identified, while larger organized domains with no long-range internal periodicity, referred to as nonperiodic lattice (NPL) crystallites,[3,22−24] have been observed experimentally. A microfibrillar structure has also been proposed as part of the silk thread structure.[25−27]

Besides the different structural elements of silk known to date, there is consensus that molecular order at different length scales is important in silk organization. Recently, with the use of mean field theory for polymers, Porter et al. have suggested a new model based on the density of hydrogen bonding between polypeptide chains to predict structure−property relationships of spider silk.[28] This model describes spider silk as a two-phase nanostructured material composed of ordered and disordered fractions (the more ordered phase containing more closely packed hydrogen bonds) that would ensure a cohesive network that can adequately store and dissipate energy.

Although spider silk has been broadly studied, the degree of order of the overall structural constituents (including crystalline and amorphous phases) has not been quantified and mapped at the nanometer scale. The domain size of oriented regions, their organization, distribution, and connectivity can all be expected to affect the mechanical properties of the silk fiber. To contribute to the refinement of existing structural models, scanning transmission X-ray microscopy (STXM) has been used to characterize the structural organization in dragline silk monofilament in terms of spatial distributions of molecular orientation. In a recent study, we have shown that it was possible to quantitatively map the level of orientation of the carbonyl bonds of the polypeptide chains at high spatial resolution (<100 nm) in *Bombyx mori* (*B. mori*) cocoon silk.[29] Since the spinning speed has been shown to affect silk mechanical properties[4,30] and, thus, the microstructure, we have used STXM to address the morphology and orientation differences of dragline silk spun at two different spinning speeds, one associated with web construction (0.5 cm/s) and the other associated with vertical descent (10 cm/s). When combined and compared with Raman measurements, STXM results give new insights on structure−property relationships in silk samples.

Methods and Materials

Fiber Samples. Spider dragline silk was collected from adult females of the *N. clavipes* species obtained from central Florida and kept in our laboratories at Université Laval under controlled conditions (25 ± 1 °C, 60 ± 5% RH, 12 h day/light cycle). The spiders were fed with crickets twice a week, and the webs were sprayed with tap water for water intake. The silk samples were obtained by forced silking on fully awake spiders. Samples were reeled at 0.5 and 10 cm/s onto glass test tubes under controlled conditions (same as mentioned above for spider farming). On the basis of the recommendations formulated by Ortlepp et al. regarding forced silking,[31] the spider was positioned vertically facing down so that the spinneret was tangential to the rotating motor, and only the silk obtained between the 5th and 15th min of forced silking was kept for analysis. The results presented herein were obtained from multiple samples silked from the same spider.

Short, adjacent segments (approximately 5 cm in length) were gently unwound from the glass tubes and transferred onto glass microscope slides with double-sided tape, stored fresh in an airtight container, and shipped immediately to McMaster University for ultramicrotomy. The procedures used previously to embed and section *B. mori* silkworm cocoon silk[29] were followed. Within 1 week of collection, the fibers were embedded in an epoxy resin made from trimethylolpropane triglycidyl ether and 4,4′-methylenebis(2-methylcyclohexylamine) in a 1:1 weight ratio and cured at 60 °C for 2 days. This epoxy does not require further sample dehydration and exhibits superior radiation resistance compared to Spurr's epoxy (resin commonly used in TEM preparations). This matrix does not contain carbonyl and phenyl groups that might interfere with the spectral analysis. Longitudinal sections

(11) Riekel, C.; Madsen, B.; Knight, D.; Vollrath, F. *Biomacromolecules* **2000**, *1*, 622−626.
(12) Termonia, Y. *Macromolecules* **1994**, *27*, 7378−7381.
(13) Grubb, D. T.; Jelinski, L. W. *Macromolecules* **1997**, *30*, 2860−2867.
(14) Simmons, A.; Ray, E.; Jelinski, L. W. *Macromolecules* **1994**, *27*, 5235−5237.
(15) Kümmerlen, J.; van Beek, J. D.; Vollrath, F.; Meier, B. H. *Macromolecules* **1996**, *29*, 2920−2928.
(16) van Beek, J. D.; Hess, S.; Vollrath, F.; Meier, B. H. *Proc. Natl. Acad. Sci. U.S.A.* **2002**, *99*, 10266−10271.
(17) Simmons, A. H.; Michal, C. A.; Jelinski, L. W. *Science* **1996**, *271*, 84−87.
(18) Yang, Z.; Grubb, D. T.; Jelinski, L. W. *Macromolecules* **1997**, *30*, 8254−8261.
(19) Riekel, C.; Vollrath, F. *Int. J. Biol. Macromol.* **2001**, *29*, 203−210.
(20) Sapede, D.; Seydel, T.; Forsyth, V. T.; Koza, M. A.; Schweins, R.; Vollrath, F.; Riekel, C. *Macromolecules* **2005**, *38*, 8447−8453.
(21) Miller, L. D.; Putthanarat, S.; Eby, R. K.; Adams, W. W. *Int. J. Biol. Macromol.* **1999**, *24*, 159−165.
(22) Thiel, B. L.; Kunkel, D. D.; Viney, C. *Biopolymers* **1994**, *34*, 1089−1097.
(23) Thiel, B. L.; Guess, K. B.; Viney, C. *Biopolymers* **1997**, *41*, 703−719.
(24) Trancik, J. E.; Czernuszka, J. T.; Bell, F. I.; Viney, C. *Polymer* **2006**, *47*, 5633−5642.
(25) Mahoney, D. V.; Vezie, D. L.; Eby, R. K.; Adams, W. W. In *Silk Polymers: Materials Science and Biotechnology*; Kaplan, D., Ed.; ACS Symposium Series 544; American Chemical Society: Washington, DC, 1994; pp 196−210.
(26) Vollrath, F.; Holtet, T.; Thogersen, H. C.; Frische, S. *Proc. R. Soc. London, Ser. B* **1996**, *263*, 147−151.
(27) Augsten, K.; Muhlig, P.; Herrmann, C. *Scanning* **2000**, *22*, 12−15.
(28) Porter, D.; Vollrath, F.; Shao, Z. Z. *Eur. Phys. J. E* **2005**, *16*, 199−206.
(29) Hernández Cruz, D.; Rousseau, M.-E.; West, M. M.; Pézolet, M.; Hitchcock, A. P. *Biomacromolecules* **2006**, *7*, 836−843.
(30) Madsen, B.; Shao, Z. Z.; Vollrath, F. *Int. J. Biol. Macromol.* **1999**, *24*, 301−306.
(31) Ortlepp, C.; Gosline, J. *Biomacromolecules* **2004**, *5*, 727−731.

of a nominal 100 nm thickness were transferred onto formvar-coated TEM grids. The formvar coating provided additional support for the sections to prevent loss of cohesion between the silk fiber and the epoxy matrix, which otherwise produced undesirable density ripples in the fiber sample. In addition, only the results from fresh sections (microtomed and measured within 2 weeks of silk collection) were used because elongated cavities have been observed to propagate along the fiber axis in older samples kept at room temperature. From our experience, freshly microtomed samples should be studied since deterioration with time (~1 month period) has been noticed. Accordingly, the choice of the best sections to be analyzed was based on a good adhesion of the fiber to the epoxy matrix, the absence of epoxy wrinkling (which often occurred because of the small thickness of the samples) to avoid constraints on the fiber sample, and a homogeneous diameter of the fiber throughout the analyzed region. Visible light microscopy (Leica Digital Module R, Leica Microsystems GmbH, Wetzlar) in reflection mode was used to choose the best sections. Fresh sections of native *B. mori* cocoon silk, supplied by the Insects Production Unit of the Canadian Forestry Service (Sault Ste. Marie, Ontario, Canada), were prepared as stated above for spider silk samples and allowed the acquisition of images at the same high spatial sampling (30 nm) that was used for the dragline silk.

STXM. X-ray imaging and spectroscopy were carried out at the Advanced Light Source using an interferometrically controlled STXM microscope at beamline 5.3.2 (STXM 5.3.2).[32,33] A nitrogen filter (pressure ~0.8 Torr over 1 m of the beamline, differentially pumped) was used to remove the X-ray beam second order. Spectra and image sequences in the C 1s region were recorded from longitudinal sections in the dry state. All data were collected with an entrance slit of 60 μm, a dispersive exit slit of 30 μm, and a nondispersive exit slit of 30 μm. The STXM tank was pumped to ~0.2 Torr and then filled with 250 Torr of He prior to measurements. The polarization dependence was obtained by mounting the sample (on a 3 mm TEM grid) on a homemade motorized azimuthal rotator[34] so that the angle of the sample relative to the electric vector (**E** vector) of the X-rays could be controlled from outside of the microscope tank. Preimaging at the selected rotation angles was used to obtain a set of coordinates, which simplified locating the region of interest after each rotation. The as-recorded transmission signals were converted to optical density (absorbance) using incident flux (I_o) signal measurements through an adjacent region of the formvar support.

The polarized near-edge X-ray absorption fine structure (NEXAFS) spectra were obtained from line scan spectra at 90° ($A_\perp$; our choice of anglular scale is such that 90° corresponds to the fiber axis aligned perpendicular to the **E** vector) and at 0° ($A_{||}$, with the fiber axis parallel to the **E** vector) recorded in the same region of the sample. The peak of interest at 288.2 eV is due to the superposition of the C 1s $\rightarrow \pi^*_{amide}$ transition (polarization sensitive) and an underlying signal (referred to as non-π* signal) that comes from other transitions associated with the protein backbone and side chains (see Figure 1). By recording an image sequence at three specific energies (287.4, 288.2, and 289.0 eV), the optical density (I) of the C 1s $\rightarrow \pi^*_{amide}$ signal could be isolated from the underlying non-π* signal by subtracting an average background image (($I_{287.4} + I_{289.0}$)/2) from the image obtained at 288.2 eV. Details concerning this method have already been published.[29] The resulting images, hereafter called polarization images, were acquired at several angles, 0, 15, 30, 54, 72, and 90°, for both the fastpull (10 cm/s) and slowpull (0.5 cm/s) fibers. All of the images were recorded with 30 nm sampling and a spatial resolution of ~45 nm.

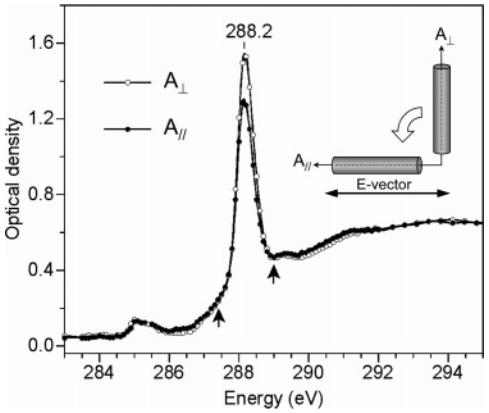

Figure 1. The C 1s near-edge X-ray absorption fine structure (NEXAFS) polarized spectra of a dragline silk fiber spun at 0.5 cm/s with the fiber axis oriented at 90 ($A_\perp$) and 0° ($A_{||}$) with respect to the electric vector of the X-ray light (see inset image). The peak at 288.2 eV is associated with the C 1s (C═O) $\rightarrow \pi^*_{amide}$ transition and shows strong linear dichroism.

The spatial resolution was determined by the zone plate used (35 nm outer-zone diameter, 165 μm diameter), the coherent content of the light (controlled by the exit slit size), and any spatial drift from image to image, which is not compensated by either the interferometry or postacquisition alignment. The polarized signal was shown to vary proportionally to a cosine-squared function and thus arises from linear dichroism. The motorized azimuthal rotator allowed reasonable control of the sample angle, but the actual angle used in fitting the results was obtained from the images themselves since the deviation between the actual and the set angle ranged from 0.2 to 4.7°. As briefly explained below and fully detailed elsewhere,[29] images obtained at 0 and 90° were used to generate the quantitative orientation maps. The experimental angle values are (−1.5, 87.1°) and (−0.5, 89.8°) for the slowpull and fastpull fibers, respectively. In the case of the *B. mori* cocoon fiber, the experimental angle values are (−2.2, −88.4°). The deviations from the ideal (0, 90°) angles were judged to be too small to justify further correction. The images were aligned so that they had the same spatial scale and pixel spacing prior to correction for the horizontal linear-polarization fraction of beamline 5.3.2, which has been measured to be 80 ± 10%.[35,36] The resulting corrected polarized images had optical densities over 0.3 clipped to get rid of the signal associated with the epoxy, which is unoriented. This clipping is arbitrary but needed to minimize the epoxy contribution and ensure that there are no negative values in the polarized images prior to division.

Since STXM is a quantitative absorption experiment, it is possible to quantify the level of orientation of the carbonyl groups from the dichroic ratio (R) of the experimental polarized images. The dichroic ratio image was obtained by dividing the 0° image ($A_{||}$) by the 90° image ($A_\perp$). For a uniaxial system such as a fiber, the dichroic ratio image can then be used to calculate a map of the order parameter, $\langle P_2 \rangle$, of the transition moments using eq 1,[37] which gives an average value of the distribution of the orientation of the structural units (carbonyls) inside the sample with respect to the reference axis (fiber axis). Image processing was carried out using aXis2000.[38]

$$\langle P_2 \rangle = \frac{R-1}{R+2} \tag{1}$$

Histograms of the $\langle P_2 \rangle$ values were then obtained from the $\langle P_2 \rangle$ quantitative maps for samples spun at different reeling speeds. These

(32) Warwick, T.; Ade, H.; Kilcoyne, A. L. D.; Kritscher, M.; Tylisczcak, T.; Fakra, S.; Hitchcock, A. P.; Hitchcock, P.; Padmore, H. A. J. *Synchrotron Radiat.* **2002**, *9*, 254−257.
(33) Kilcoyne, A. L. D.; Tyliszczak, T.; Steele, W. F.; Fakra, S.; Hitchcock, P.; Franck, K.; Anderson, E.; Harteneck, B.; Rightor, E. G.; Mitchell, G. E.; Hitchcock, A. P.; Yang, L.; Warwick, T.; Ade, H. *J. Synchrotron Radiat.* **2003**, *10*, 125−136.
(34) Hernández Cruz, D.; Hitchcock, A. P.; Tyliszczak, T.; Rousseau, M.-E.; Pézolet, M. *Rev. Sci. Instum.* **2006**, in press.
(35) Watts, B.; Thomsen, L.; Dastoor, P. C. *J. Electron Spectrosc. Relat. Phenom.* **2006**, *151*, 208−214.
(36) Watts, B.; Ade, H. *J. Electron Spectrosc. Relat. Phenom.* **2007**, submitted.
(37) Buffeteau, T.; Pézolet, M. Linear Dichroism in Infrared Spectroscopy. In *Handbook of Vibrational Spectroscopy*; Chalmers, J. M., Griffith, P. R., Eds.; John Wiley and Sons: West Sussex, U.K., 2002; Vol. 1, pp 693−710.
(38) aXis2000 is written in Interactive Data Language (IDL). It is available free for noncommercial use from http://unicorn.mcmaster.ca/aXis2000.html.

curves were normalized to the same area to account for the differing number of pixels in the two different fibers analyzed since the fiber diameter varies with reeling speed. Values of the maximum, average, and standard deviations for each histogram were obtained using GRAMS/AI 7.0 and Microsoft Excel. For the color coding, fixed colorization intervals were chosen with ranges based on the statistics of the $\langle P_2 \rangle$ distributions. The images were colored at the pixel level with both aXis2000 and Photoshop 7.0 (Adobe System Incorporated, 1990−2002). The domain sizes and size distributions were calculated with Image Pro Plus 4.0.0.13 (Media Cybernetics. L.P., 1993−1998).

Results and Discussion

Dichroism Effect. Figure 1 presents characteristic C 1s NEXAFS spectra of a longitudinal section of *N. clavipes* dragline silk recorded with the **E** vector perpendicular and parallel to the fiber axis (see the inset image for the two orientations). These spectra were obtained for the fiber spun at 0.5 cm/s, but the spectral features discussed herein were very similar for the sample spun at 10 cm/s. The C 1s spectrum of proteins is dominated by an intense absorption peak at 288.2 eV associated with the C 1s (C═O) → π^*_{amide} transition. The transition-moment vector for this absorption band is perpendicular to the plane of the peptide bond.[39,40] As seen in Figure 1, this band shows strong linear dichroism, as it is more intense when the fiber axis is oriented perpendicular to the **E** vector. A similar polarization dependence was also observed for the cocoon silk spun by the silkworm *B. mori*.[29] Since STXM is an absorption experiment, the band intensity should vary with the square of the cosine of the angle between the transition moment and the incident electric vector. This polarization dependence has been verified with the acquisition of polarized images at several angles (see the Methods and Materials). Thus, it can be concluded from the spectra in Figure 1 that the transition moments associated with the peak at 288.2 eV are preferentially oriented perpendicular to the fiber axis. This result is in good agreement with polarized Raman spectra obtained for the same type of silk, which shows a strong polarization effect for the amide I band which is mainly due to the stretching vibration of the amide carbonyl group.[41−43]

In a typical acquisition by STXM, images are obtained at many sequential energies so that each pixel in the image sequence contains the full spectrum. This constitutes a major advantage of spectromicroscopy, whereby each component of an imaged region (within the spatial resolution limitations of the apparatus) can be spectroscopically identified and its spatial distribution mapped quantitatively. However, a compromise has to be made between several factors: (i) the size of the analyzed region (it has to be large enough to get a good view of the sample morphology), (ii) the measurement time (limited while doing synchrotron experiments), and (iii) the total radiation dose to be put into the sample without degradation. Since silk fibers are essentially composed of pure spidroin proteins, recording full-image sequences (i.e., the full spectral range shown in Figure 1) does not provide significant additional information. On the basis of the results obtained on *B. mori* cocoon silk,[29] images at only three energies, 288.2, 287.4, and 289.0 eV, corresponding to the peak maximum showing dichroism, pre-edge, and post-edge, respectively (see Figure 1), are sufficient for generating quantitative maps of the dichroic signal linked to the molecular orientation. The image measured at 288.2 eV, which contains the polarization-dependent information (π^*_{amide} signal), was corrected for the unpolarized background signal (non-π^* signal), as described in the Methods and Materials section. The resulting image, hereafter called a polarization image, only contains the π^* signal. Examples of polarization images obtained at 0 and 90° are shown in Figure 2, presented on a common optical density grayscale. There is a significant difference in the intensity level between the 0 and 90° polarization images. In agreement with the spectra shown in Figure 1, the brighter image is obtained when the fiber is perpendicular to the **E** vector, thus indicating greater absorptivity in that polarization. For both images, the bottom part of the fiber is slightly brighter, by ∼10%. This effect is clearly due to density or thickness variations across the fiber, which could be either natural or due to microtoming, since it disappears in the image ratio (see the $\langle P_2 \rangle$ image in Figure 3.

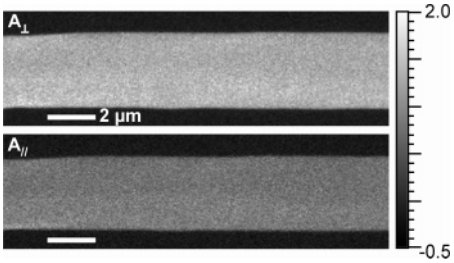

Figure 2. Polarization images of a dragline silk fiber spun at 0.5 cm/s with the fiber axis oriented at 90 ($A_\perp$) and 0° ($A_{//}$) with respect to the electric vector of the X-ray light. The brighter image is obtained at 90°, thus indicating greater absorptivity in this polarization and preferential orientation of the carbonyl groups perpendicular to the fiber axis.

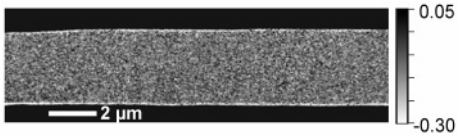

Figure 3. Quantitative $\langle P_2 \rangle$ orientation map of the slowpull fiber (0.5 cm/s). Black areas correspond to unoriented regions, whereas bright areas correspond to more highly oriented regions. The limiting values of $\langle P_2 \rangle$ are 1 and −0.5 for perfect orientation of the transition-moment vector at 0 and 90° from the fiber axis, respectively.

Quantitative Orientation Map. As shown previously for *B. mori* cocoon silk,[29] the 0 and 90° polarization images can be converted to $\langle P_2 \rangle$ maps of the orientation of the carbonyl groups. The resulting map obtained for the slowpull fiber (0.5 cm/s) is presented in Figure 3. Note that, compared to the polarization images (Figure 2), the grayscale is reversed; bright areas in the $\langle P_2 \rangle$ map correspond to more highly oriented regions, whereas black areas correspond to unoriented regions. With a spatial resolution of 45 nm, one can appreciate the very fine nanostructure of oriented regions in dragline silk. According to a recent structural model,[28] the stiffness and toughness values found in spider silk would necessitate a nanoscale morphology to allow the energy to be efficiently shared between ordered and disordered domains, which is in good agreement with our results.

(39) Stöhr, J.; Outka, D. *Phys. Rev. B* **1987**, *36*, 7891−7905.
(40) Croll, L. M.; Britten, J. F.; Morin, C.; Hitchcock, A. P.; Stover, H. D. H. *J. Synchrotron Radiat.* **2003**, *10*, 265−268.
(41) Gillepsie, D. B.; Viney, C.; Yager, P. In *Silk Polymers: Materials Science and Biotechnology*; Kaplan, D., Ed.; ACS Symposium Series 544; American Chemical Society: Washington, DC, 1994; pp 155−167.
(42) Rousseau, M.-E.; Lefèvre, T.; Beaulieu, L.; Asakura, T.; Pézolet, M. *Biomacromolecules* **2004**, *5*, 2247−2257.
(43) Lefèvre, T.; Rousseau, M.-E.; Pézolet, M. *Biophys. J.* **2006**, *92*, in press.

Although spider silk has been long considered as a semicrystalline biopolymer, our results obtained on different monofilaments having a length of a few tens of microns did not present either visible regular lamellar structure or any periodicity along the fiber axis in terms of molecular orientation (considering either crystalline or amorphous regions). The oriented domains observed in Figure 3, which range from 900 to 5400 nm^2 (corresponding to an area of 1−6 pixels, where the size of 1 pixel is 30 nm x 30 nm), are too large to be associated with individual β-sheet crystallites, which are known to be smaller than 10 nm, as determined by wide-angle X-ray scattering.[13] Even by adding an interphase of a few nanometers around the crystallites as suggested by Termonia's model,[12] the given dimensions are not sufficient to account for the area of the oriented domains observed experimentally. From this result, the microstructure of the spider silk fiber could be more appropriately described by chain assembly based on interactions of neighboring polypeptide chains through interchain hydrogen bonds. Recent neutron scattering experiments have supported the presence of nanofibrils that have a rod-like structure with a maximum length of 170 nm.[20] Since the width of such fibrils is clearly below the spatial resolution currently achievable by STXM, they could not be visualized. However, the fact that the STXM $\langle P_2 \rangle$ maps unambiguously show the presence of domains with variable degrees of orientation indicates that the nanofibrils are not homogeneously distributed in the fibers but are rather clustered into larger oriented domains (30−100 nm range). Another possible interpretation of the STXM results is the NPL model proposed for silk organization by Thiel et al.,[22] which is also found in solidified liquid crystalline copolyesters that are stabilized by random matches between locally compatible domains on adjacent chains. Accordingly, such an organization would allow formation of a hydrogen-bond network that would account for spider silk's mechanical properties, as suggested by a recent structural model.[28] Bundles of 3_1 helices have also been suggested to be present in the fiber core by NMR spectroscopy.[15,16] According to molecular models, the carbonyl groups in this helical conformation are almost perpendicular to the helix axis. Therefore, the carbonyl groups of helices oriented along the fiber axis would also contribute to the observed STXM dichroic signal.

Knowing that the limiting values of $\langle P_2 \rangle$ are 1 and −0.5 for perfect orientation of the transition-moment vector at 0 and 90° from the fiber axis, respectively, the $\langle P_2 \rangle$ map shown in Figure 3 indicates, quantitatively, that the transition moments are preferentially oriented perpendicular to the fiber axis. There is clearly an uneven spatial distribution of highly oriented (bright) domains, especially at the surface of the fiber where a skin ∼30−120 nm thick is present. This morphological feature has been observed by electron microscopy[27,44,45] and was shown to vary within 150 to 250 nm.[27] Fluorescence measurements, combined with the use of Congo red, which is a dye that specifically bonds to antiparallel β-sheets,[46] have shown a higher β-sheet content at the surface of the fiber, presumably caused by high extensional flow stresses occurring in the spinning apparatus.[10] The current STXM results further demonstrate that the β-sheet domains observed in the skin of dragline silk (Figure 3) are relatively large, continuous, and highly oriented. This peculiar skin effect seems to be due to the spinning itself but might also be a factor in determining the mechanical properties of the silk filament. In comparison, highly oriented crystallites have also been observed in the skin region of high-modulus polymeric fibers such as poly(*p*-phenylene terephthalamide) (PPTA, also known as Kevlar)[47−49] and poly(*p*-phenylene benzobisoxazole) (PBO).[50] Shear forces occurring during spinning contribute to increase the alignment of the chains and are considered responsible for this effect.

Effect of Spinning Speed on $\langle P_2 \rangle$ Distributions. It has been observed that spiders spin their dragline silk over a wide range of spinning speeds depending on the function of the resulting thread. Silk used for building the web frame is spun rather slowly (<1 cm/s), while silk used for a rapid vertical descent to elude a predator is spun at least 1 order of magnitude faster (>10 cm/s). It has been shown that the speed at which a silk filament is spun affects its mechanical properties and certainly changes its microstructure.[4,30] Interestingly, quantitative Raman measurements on samples spun at different speeds (0.5, 2, and 10 cm/s) (unpublished data) have revealed no significant differences in the amount and level of orientation of the β-sheets in dry silk samples (20% RH as opposed to samples studied at 60% RH). It is, therefore, of great interest to further investigate the microstructure differences at high spatial resolution in these samples. We emphasize that the results shown in the present study were obtained on silk samples that came from the same spider, on the same day, under controlled experimental conditions.

Figure 4A shows superimposed histograms derived from the $\langle P_2 \rangle$ orientation maps that have been normalized for the same area under the curve to account for different fiber diameters, as discussed below. These histograms show that the majority of the pixels composing the $\langle P_2 \rangle$ orientation maps for both spinning speeds have negative values, with average values of -0.14 ± 0.06 and -0.14 ± 0.04 for the slowpull and fastpull fibers, respectively. The average negative $\langle P_2 \rangle$ values indicate that, globally, the molecular chains have a predominant alignment toward the fiber axis. Similar conclusions have been derived from NMR measurements on labeled silk samples.[16] Moreover, recent Raman measurements have determined an average $\langle P_2 \rangle$ of -0.24 ± 0.02 for *N. clavipes* silk by considering the order parameters of different secondary structures weighted for their respective proportion in silk.[43] These findings imply that the orientation of the bulk, referred to as the noncrystalline or amorphous fraction in silk, has been underestimated in numerous structural models that have attempted to explain the mechanical properties of spider silk. It is, however, highly possible that this portion of the matrix would have a lower level of orientation in the case of a humidified fiber.

Although the average level of orientation of the polypeptide chains is similar for both reeling speeds, the histograms exhibit major differences. The distribution of orientation of the

(44) Li, S. F. Y.; McGhie, A. J.; Tang, S. L. *Biophys. J.* **1994**, *66*, 1209−1212.
(45) Frische, S.; Maunsbach, A. B.; Vollrath, F. *J. Microsc. (Oxford, U.K.)* **1998**, *189*, 64−70.
(46) Taylor, D. L.; Allen, R. D.; Benditt, E. P. *J. Histochem. Cytochem.* **1974**, *22*, 1105−1112.
(47) Panar, M.; Avakian, P.; Blume, R. C.; Gardner, K. H.; Gierke, T. D.; Yang, H. H. *J. Polym. Sci.* **1983**, *21*, 1955−1969.
(48) Morgan, R. J.; Pruneda, C. O.; Steele, W. J. *J. Polym. Sci.* **1983**, *21*, 1757−1783.
(49) Young, R. J.; Lu, D.; Day, R. J.; Knoff, W. F.; Davis, H. A. *J. Mater. Sci.* **1992**, *27*, 5431−5440.
(50) Davies, R. J.; Montes-Morán, M. A.; Riekel, C.; Young, R. J. *J. Mater. Sci.* **2003**, *38*, 2105−2115.

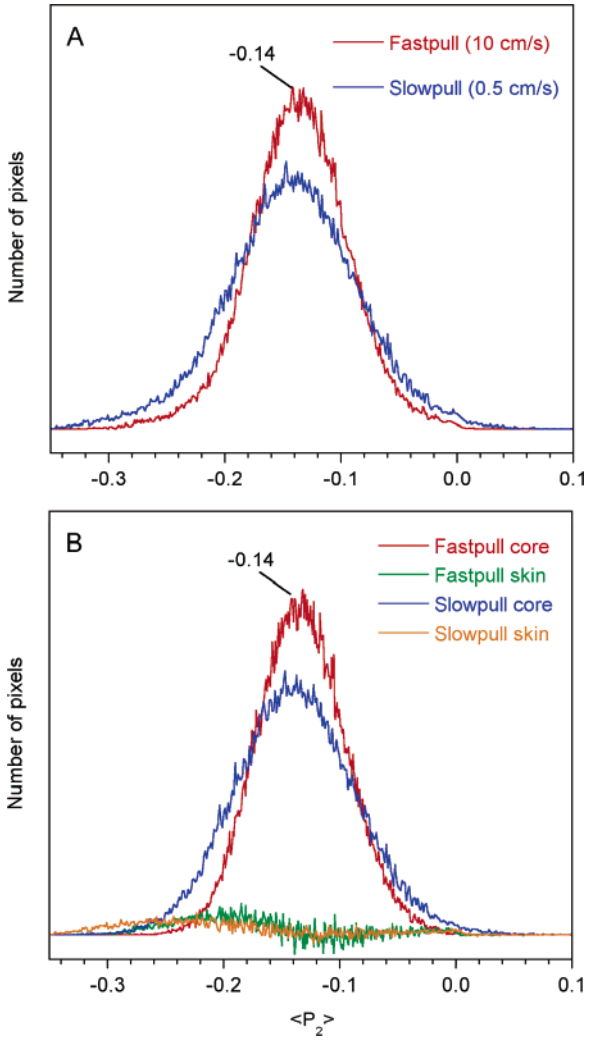

Figure 4. (A) Histograms of the $\langle P_2 \rangle$ values obtained for the dragline samples spun at 0.5 and 10 cm/s. The intensity of the distributions were normalized to give the same area under the curves. (B) Skin and core distributions of dragline samples spun at 0.5 and 10 cm/s. The skin distributions are those of pixels within 120 nm of the edge.

carbonyls in the slowpull fiber presents a clear shoulder for a high negative $\langle P_2 \rangle$ that is associated with the skin region, as discussed above. To highlight the effect of the skin on the distribution of $\langle P_2 \rangle$, the orientation distributions corresponding to the skin (within 120 nm of the edge) and core regions are presented separately in Figure 4B. As can be seen, the core distributions are nearly Gaussian in shape, although some tailing appears for high values of $\langle P_2 \rangle$ (low level of orientation). However, the fiber spun at 10 cm/s shows a narrower distribution that could be interpreted as a general increase in the quality of the alignment of the polypeptide chains, thus reducing the number of defects present and producing a stiffer fiber (observed experimentally; data not shown). Increases of the tensile strength with increasing reeling speed have also been observed elsewhere.[4,30] In situ X-ray diffraction measurements on as-spun silk filaments have demonstrated that increasing the spinning speed positively affected the level of molecular orientation,[4,11] in good agreement with a narrower distribution when the fiber is spun at 10 cm/s. It is clear from Figure 4B that the skin of both the fastpull and slowpull fibers is composed of more highly oriented chains than those present in the core. These results strongly suggest a bimodal orientation distribution that could

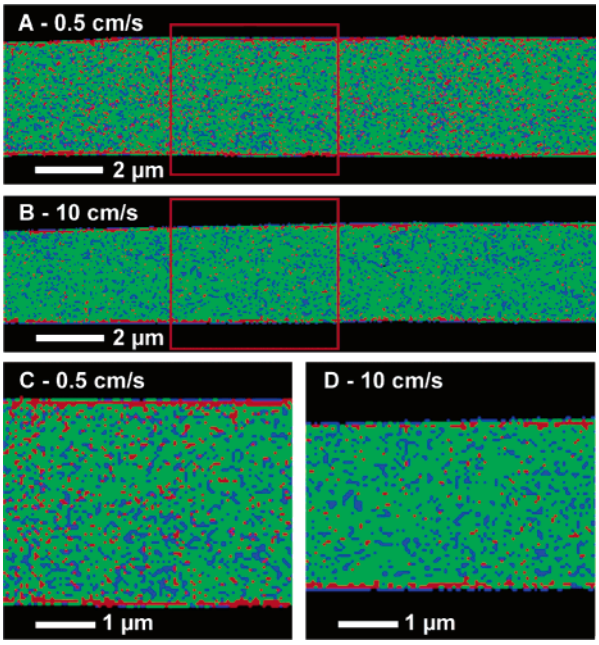

Figure 5. Color-coded $\langle P_2 \rangle$ maps of spider dragline from *N. clavipes* spun at two different spinning speeds based on fixed intervals: highly oriented regions in red ($\langle P_2 \rangle < -0.19$), moderately oriented regions in green ($[-0.19 \leq \langle P_2 \rangle \leq -0.09]$), and unoriented regions in blue ($\langle P_2 \rangle > -0.09$). (A−B) Full region 18 μm in length. (C− D) Expanded region 5 μm wide, corresponding to the framed sections in A and B.

be linked to the existence of two fractions of crystallinity, a phenomenon that has been observed by wide-angle[51] and small-angle X-ray scattering[18] and incorporated in the schematic model derived from NMR data.[17]

To further explore the spatial distribution of the $\langle P_2 \rangle$ values and highlight the presence of highly and slightly oriented domains, color maps were constructed based on colorization of fixed intervals, determined by the statistics of the two histograms shown in Figure 4A. Figure 5 presents color-coded $\langle P_2 \rangle$ maps of dragline fibers obtained at the two spinning speeds (0.5 and 10 cm/s) over the full region studied (A and B) and in a zoomed section of a 5 μm width (C and D). As seen in this figure, the silk fiber diameter is greatly effected by the reeling speed. Decreases in fiber diameter with increasing spinning speed have also been observed by Vollrath et al.[4] Since the spider spinning apparatus is more likely to have a fixed throughput of silk proteins during spinning, the increasing spinning speed results in the lowering of the filament linear density, which causes a decrease of the fiber cross-sectional area.[52] The breaking strain and the fiber's toughness were also found to decrease in filaments obtained at higher spinning speed. The first interval colored in green corresponds to the $\langle P_2 \rangle$ values within plus or minus one standard deviation of the average ($[-0.19 \leq \langle P_2 \rangle \leq -0.09]$). The highly oriented domains ($\langle P_2 \rangle < -0.19$) are colored in red, while the least oriented pixels ($\langle P_2 \rangle > -0.09$) are colored in blue. Relatively long sections of the fibers have been analyzed (18 μm in length) to examine the fiber microstructure over large areas at the submicron scale. At this level of spatial resolution (using 30 nm pixels and ~45 nm spatial resolution) on samples that are relatively thin (100 nm

(51) Riekel, C.; Braenden, C.; Craig, C.; Ferrero, C.; Heidelbach, F.; Mueller, M. *Int. J. Biol. Macromol.* **1999**, *24*, 179−186.
(52) Raghavan, J. S.; Cuculo, J. A. *J. Polym. Sci., Part B: Polym. Phys.* **1999**, *37*, 1565−1573.

thick), no pattern was apparent. Besides the fact that the density of oriented and unoriented domains is greater in the slowpull sample, the green region is the major component of the fiber core in both cases. It represents 81% of the pixels of the fastpull fiber but only 68% in the slowpull fiber. This indicates that chains composing the bulk of the fiber are slightly oriented parallel to the fiber axis with an average $\langle P_2 \rangle$ of -0.14. The relatively high level of orientation of the molecular chains in the bulk must play a critical role in stress transfer between highly oriented domains. A skin with a thickness varying between 30 and 120 nm composed of highly oriented chains is clearly seen for both fibers. However, the effect seems to vary with the spinning speed and appears to be more important for the slowpull fiber. On the other hand, according to the stress-induced crystallization theory in polymers, crystallization occurs due to local stresses which increase with increasing spinning speed.[52] Therefore, our results suggest that local stresses are not the major factor responsible for crystallization of the proteins on the surface of the fiber, although the high extensional flow stresses occurring at the draw-down taper in the spinning apparatus have been suggested to be responsible for a skin effect.[10] In polymers, the skin crystallization effect occurs because of the temperature gradient during spinning, especially close to the spinneret. However, other factors such as protein dehydration or local pH gradients might be involved in skin formation in silk fibers. Another possible explanation for the skin to become less apparent in the fastpull fiber is that the domain size is getting closer to the spatial resolution of STXM as the fiber diameter decreases with spinning speed.

The analysis of the color-coded maps further reveals that the average area of each highly oriented domain (red region) is under 4 pixels (<3600 nm^2) for both spinning speeds but that the pixel fraction corresponding to these domains doubles from 8 to 17% between the fastpull and slowpull fibers, respectively. Based on quantitative Raman measurements, the β-sheet content of *N. clavipes* dragline has been estimated to be $37 \pm 3\%$.[43] Since the present results indicate that only 17% of the pixels have a $\langle P_2 \rangle$ value lower than -0.19, this implies that a fraction of the β-sheets must be less oriented, in agreement with NMR results that have shown the presence of two populations of β-sheets.[17] In addition to highly oriented domains, a non-negligible number of pixels are present which show a low level of orientation. The blue regions, which have an average area under 5 pixels (<4500 nm^2), are more abundant in the slowpull fiber and represent a pixel fraction of 15% compared to 11% for the fastpull fiber.

A quantitative analysis of the domain sizes has been carried out to evaluate the effect of the spinning speed on the size of the organized entities found in the silk core (the pixels of the skin within 120 nm of the edge were rejected for this analysis). The results indicate that most of the highly oriented domains found in the fastpull fiber (98%) have an area of one or two pixels (average area equal to or lower than 1800 nm^2). Such small domains represent 87% of all of the oriented domains in the slowpull fiber. It is to be noted that the present data do not exclude the possibility that other structures may be present at a smaller scale and could not be detected in the present experiment. It is, however, clear that the oriented domains are larger in the slowpull fiber since 4% of the domains found have an area equal to or greater than 5 pixels (4500 nm^2), while this size distribution is found in less than 1% in the fastpull fiber. This result is in good agreement with TEM results that have shown that diffracting objects, referred to as NPL crystals, were smaller in the fiber spun at 10 cm/s.[3] Indeed, Thiel and co-workers[23] have proposed from TEM measurements that the highly oriented domains observed experimentally are irregular in shape, uniformly distributed in the matrix, and 70−100 nm in diameter.[22] It is, therefore, tempting to associate the NPL diffracting objects with the highly oriented domains observed in the STXM-derived $\langle P_2 \rangle$ maps. It is also possible that these domains come from the inhomogeneous distribution of nano-sized fibrils. On the basis of either of these two organization models, we can speculate that the rate at which the fiber is spun will affect the time available for spidroin molecules or rod-like structures to organize with adjacent chains in the spinning duct and, therefore, influence the size of the organized domains found in the final thread. It is, however, clear that organized oriented domains observed herein are larger than individual β-sheet crystallites.[13] Although crystallinity is desirable to generate high modulus fibers, it has been suggested that three-dimensional order is not a prerequisite and that closely packed oriented molecular chains (high packing density) would account for the high tensile modulus of silk fibers.[53]

One could argue that the colored $\langle P_2 \rangle$ intervals were chosen arbitrarily (average $\pm$ standard deviation). However, this approach helps to visualize the spatial distribution, size, and connectivity of oriented and organized domains. The generally accepted structural model for silk[12] states that small, highly oriented crystallites are dispersed in an "amorphous" matrix. The microstructural organization revealed by our results allows the refinement of this model in that the highly oriented domains are larger than individual crystallites, the bulk of the silk core is moderately oriented, and a nonnegligible number of unoriented domains are present. Note that, in most cases, the highly oriented and unoriented domains are surrounded by a moderately oriented matrix, which would allow for good connectivity and indicates the presence of a long-range order necessary to explain silk mechanical properties. This study was performed without rigorous control of relative humidity, and therefore, it is most likely that the fiber is less hydrated than its natural state. It is possible that the level of orientation of structural elements would be different in the fully hydrated state. Measurements are under way to try to verify that assumption. However, neutron experiments have shown that certain regions are more accessible to water but that water absorption does not modify the morphology significantly.[20]

Comparison between Silkworm Cocoon and Spider Dragline Silks. Considering that STXM measurements give the opportunity to describe the silk microstructure in terms of molecular orientation, it is informative to qualitatively and quantitatively compare the present results to those obtained from the analysis of silkworm cocoon silk to clearly highlight the microstructural differences between both types of silks. From our previous paper,[29] oriented domains in cocoon silk could be easily resolved, with a pixel sampling of 100 nm. For proper comparison, additional measurements were done on freshly microtomed cocoon silk to generate an orientation map of a

(53) Kroschwitz, J. I.; Mark, H. F.; Bikales, N. M.; Overberger, C. G. High Modulus Fiber. *Encyclopedia of Polymer Science and Engineering*; Wiley-Interscience: New York, 1987; Vol. 7, pp 699−721.

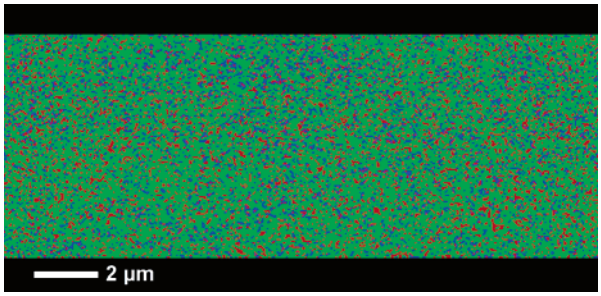

Figure 6. Color-coded $\langle P_2 \rangle$ map of one fibroin filament from the *B. mori* cocoon fiber based on fixed intervals: highly oriented regions in red ($\langle P_2 \rangle < -0.16$), moderately oriented regions in green ($[-0.16 \leq \langle P_2 \rangle \leq -0.10]$), unoriented regions in blue ($\langle P_2 \rangle > -0.10$).

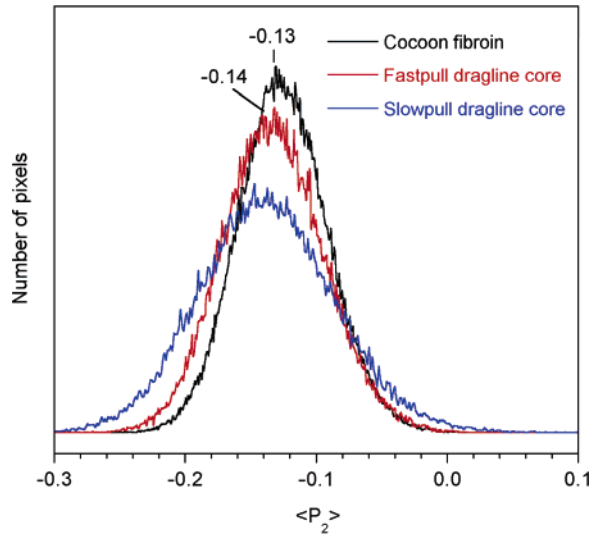

Figure 7. Comparison of the histograms of the $\langle P_2 \rangle$ values obtained for the core regions of *B. mori* cocoon fiber and spider dragline silks from *N. clavipes* spun at two different spinning speeds (fastpull, 10 cm/s; slowpull, 0.5 cm/s). The intensity was normalized to give the same area under the curves.

native *B. mori* cocoon fiber at the same spatial resolution and pixel sampling as the spider silk samples. $\langle P_2 \rangle$ data from one fibroin thread is presented in Figure 6. It was colored based on the same approach used for spider silk images. The average $\langle P_2 \rangle$ for this cocoon fiber is -0.13 ± 0.03. The data obtained at high spatial sampling reveal a much finer microstructure for cocoon silk than that detected previously using larger pixel sizes. The highly oriented domains ($\langle P_2 \rangle < -0.16$) represent only 12% of the entire fibroin core and have similar dimensions to that observed in spider silk (average area of 2 pixels or 1800 nm^2). In terms of size distribution, 80% of the highly oriented domains have an area between 1 and 2 pixels (from 900 to 1800 nm^2), a fraction comparable to that observed for slowpull spider silk (87%).

Although the size distribution of the highly oriented domains is similar in both types of silk studied, their orientation distributions show major differences. The histograms derived from the orientation maps were normalized to the area under the curve and are presented in Figure 7. The maxima on each curve occur at similar values of $\langle P_2 \rangle$, -0.14 for the slowpull dragline, -0.14 for the fastpull dragline, and -0.13 for the cocoon silk, respectively. The orientation distribution is narrower in the case of *B. mori* native fiber, which exhibits a nearly Gaussian distribution. This more homogeneous alignment of the chains in the *B. mori* fiber is consistent with it being a stiffer fiber. Figure 7 also shows that the orientation distribution for the *N. clavipes* fibers is asymmetric, particularly in the case of the slowpull sample, and skewed toward more negative $\langle P_2 \rangle$, corresponding to larger amounts of more highly oriented domains in spider dragline relative to those in cocoon silk. These dispersed, highly ordered regions could act as reinforcement features in both cases. The wider distribution as well as the larger fraction of more oriented domains found in spider silk certainly accounts for the good combination of stiffness and extensibility found in spider dragline silk. Our results clearly reveal that these two types of silk have significantly different microstructures. It thus emphasizes the fact that one must be careful when applying the same structural model to both types of silk.

Conclusions

The orientation maps obtained by STXM have allowed a new morphological characterization of spider dragline silk. The orientation maps obtained at high spatial resolution (45 nm, with 30 nm sampling) revealed a very fine structure where small, highly oriented domains (average area under 4 pixels or inferior to 3600 nm^2) are dispersed within a moderately oriented matrix with small unoriented zones (average area under 5 pixels or inferior to 4500 nm^2). The highly oriented domains are clearly larger than individual crystallites and suggest the assembly or close proximity of organized structural elements, which could be either molecular chains or fibrillar entities.

A skin-core effect was previously observed by electron microscopy using particular staining techniques.[27,44,45] However, the present data, measured on unstained samples, constitute the first experimental evidence that the polypeptide chains are more highly oriented at the surface of the fiber. Our results obtained on samples spun at different spinning speeds (0.5 and 10 cm/s) clearly reveal that the spinning speed does not have a significant effect on the average level of orientation of the chains (in agreement with quantitative Raman measurements on the β-sheets). However, the STXM results do show that the spinning speed does strongly affect the fiber microstructure. The skin-core effect was found to vary with the reeling speed and appears to be more important for the slowpull fiber. By increasing the spinning speed, the orientation distribution of the polypeptide chains becomes narrower, thus leading to a stiffer fiber which can better support the spider body weight when it attempts a vertical descent. On the other hand, the high density of highly and unoriented domains homogeneously dispersed in the fiber core of the slowpull fiber provides an interdigitated network that ensures good energy dissipation in the web structure. In comparison, the silkworm cocoon fibroin presents no particular skin structures and the more homogeneously organized protein chains lead to a stiffer but less extensible fiber.

Acknowledgment. This research was supported by the Natural Science and Engineering Research Council (NSERC, Canada), Canada Foundation for Innovation, and the Canada Research Chair programs. Construction and operation of the STXM 5.3.2 microscope is supported by NSF DMR-9975694, DOE DE-FG02-98ER45737, Dow Chemical, NSERC, and the Canada Foundation for Innovation. We thank David Kilcoyne and Tolek Tyliszczak for their contributions to developing and

maintaining the instrument. The Advanced Light Source is supported by the Director, Office of Energy Research, Office of Basic Energy Sciences, Materials Sciences Division of the U.S. Department of Energy, under Contract No. DE-AC03-76SF00098. We thank Benjamin Watts for assisting us with measurements of the polarization efficiency of beamline 5.3.2 and Thierry Lefèvre and Rodicca Plesu for their help and useful discussions.

JA067471R